Clim. Past Discuss., 4, 859–895, 2008
www.clim-past-discuss.net/4/859/2008/

Climate of the Past Discussions

Climate of the Past Discussions is the access reviewed discussion forum of *Climate of the Past*

Constraining atmospheric CO_2 content during the Middle Miocene Antarctic glaciation using an ice sheet-climate model

P. M. Langebroek[1], **A. Paul**[1,2], **and M. Schulz**[1,2]

[1]Faculty of Geosciences, University of Bremen, Bremen, Germany
[2]MARUM – Center for Marine Environmental Sciences, Univ. of Bremen, Bremen, Germany

Received: 17 July 2008 – Accepted: 28 July 2008 – Published: 12 August 2008

Correspondence to: P. M. Langebroek (petra@palmod.uni-bremen.de)

Published by Copernicus Publications on behalf of the European Geosciences Union.

Abstract

Foraminiferal oxygen isotopes from deep-sea sediment cores suggest that a rapid expansion of the Antarctic ice sheet took place in the Middle Miocene around 13.9 million years ago (Ma). The origin for this transition is still not understood satisfactorily. Among the proposed causes are a drop in the partial pressure of atmospheric carbon dioxide (pCO_2) in combination with orbital forcing. An additional complication is the large uncertainty in the magnitude and age of the reconstructed pCO_2 values and the low temporal resolution of the available record in the Middle Miocene. We used an ice sheet-climate model with an energy and mass balance module to assess variations in ice-sheet volume induced by pCO_2 and insolation forcing and to better constrain atmospheric CO_2 in the Middle Miocene. The ice-sheet sensitivity to atmospheric CO_2 was tested in several scenarios using constant pCO_2 forcing or a regular decrease in pCO_2. Small, ephemeral ice sheets existed under relatively high atmospheric CO_2 conditions (between 400–450 ppm), whereas more stable, large ice sheets occurred when pCO_2 is less than 400 ppm. Transitions between the states were largely CO_2-induced, but were enhanced by extremes in insolation. In order to explain the Antarctic glaciation in the Middle Miocene as documented by the oxygen isotope records from sediment cores, pCO_2 must have decreased by approximately 150 ppm in about 30 ka, crossing the threshold pCO_2 of 400 ppm around 13.9 Ma. Forcing the ice sheet-climate model with cyclic pCO_2 variations at a period of 100 ka and amplitudes of approximately 40 ppm generated late Pleistocene glacial-interglacial like ice-volume variations, where the ice volume lagged pCO_2 by 11–16 ka.

1 Introduction

In the Middle Miocene, around 13.9 million years ago (Ma), a large shift towards heavier benthic oxygen isotope values ($\delta^{18}O$) is found in deep-sea sediment records (Zachos et al., 2001; Holbourn et al., 2005). This increase coincided with a global sea-level

CPD

4, 859–895, 2008

drop (Miller et al., 1998, 2005) and is interpreted as an expansion of the Antarctic ice cap and a global transition into a colder climate (e.g., Zachos et al., 2001; Shevenell et al., 2004). Several causes for the transition are proposed, ranging from the effect of ocean circulation and gateways (e.g., Flower and Kennett, 1995), enhanced chemical weathering and burial of organic matter (e.g., Raymo, 1994), to orbital forcing in combination with variations of partial pressure in the atmosphere (pCO_2) (Holbourn et al., 2005, 2007). A remarkable difference of this glaciation with respect to previous large-scale events (e.g. the Eocene-Oligocene transition; Coxall et al., 2005; Pollard and DeConto, 2005) is the relatively small decline in atmospheric CO_2, varying only in the order of 100–200 ppm (cf., Pearson and Palmer, 2000; Royer et al., 2001; Pagani et al., 2005; Kürschner et al., 2008; Zachos et al., 2008). This raises questions about the origin of the Middle Miocene transition. Was orbital forcing by itself sufficient to cause a large-scale continental glaciation? Or was some additional reduction of atmospheric CO_2 needed? And if so, how large and how quick was this pCO_2 drop? Considering the large uncertainties in the most recent pCO_2 reconstructions for the Middle Miocene (Pearson and Palmer, 2000; Royer et al., 2001; Pagani et al., 2005; Kürschner et al., 2008; Zachos et al., 2008), this study aims to give constrains on for timing, duration and speed of the pCO_2 transition using a modelling approach. We examine these questions using a geometrically simplified, but physically comprehensive ice sheet-climate model, which is forced by insolation (derived from the orbital parameters) and atmospheric CO_2 only.

2 Methods and experimental set-up

2.1 Ice sheet-climate model

We used a coupled ice sheet-climate model. The climate component consists of three large-scale boxes covering the entire southern hemisphere: a low (0–30° S), middle (30–60° S) and high (60–90° S) latitude box (Fig. 1). Forcing consists of seasonal or-

bital forcing following the work of Laskar et al. (2004) in combination with prescribed atmospheric CO_2 levels. In the large-scale boxes of the climate model, energy is conserved and is redistributed by meridional energy transport, taking into account the latent heat fluxes due to evaporation and snow accumulation. The physical processes within the high latitude box are resolved in 0.5° latitude bands. In these boxes energy balances the for atmosphere and surface are resolved separately, but computed simultaneously. Additionally, the mass balance for the ice-sheet component is modeled. Daily computation is necessary, because the orbital cycle as well as processes of snow accumulation and melting have a strong seasonal imprint (Pollard, 1983).

The atmospheric and surface energy balances include parameterizations for short- and longwave radiation, latent heat of evaporation and snowfall, sensible heat exchange, heat flux into the surface and energy used by melting of ice and snow (Pollard, 1982, 1983; Jentsch, 1987, 1991; Wang and Mysak, 2000). Total accumulation and its latitudinal distribution is tuned to the present-day (total) Antarctic accumulation and depends on surface temperature, distance from the coast, surface height and daily surface temperature (Oerlemans, 2002, 2004). It therefore includes important processes such as the elevation-desert effect (Pollard, 1983). The ice-sheet model is symmetric around the axis of the South Pole. Within the ice sheet velocities and temperatures are computed with a vertical resolution of 12 layers. The altitude and ice thickness of every latitude grid cell are derived by solving the continuity equation using basal melting, local bedrock isostasy and a surface mass balance (Sima, 2005; Sima et al., 2006). The initial ice-free bedrock topography is reconstructed using the BEDMAP project database (Lythe et al., 2000) for bedrock elevation and ice thickness, considering local isostasy. For the axially symmetric ice-sheet model, the high spatial resolution of the dataset is reduced, averaging the topography into the 0.5° -wide latitude bands. The initial bedrock used by the model is a simplified version of the zonally-averaged topography that includes a bulge close to the continental shelf and a flatter hinterland. Although no separate ocean component is included in the model, the energy and mass balances within the Antarctic box include the albedo of (seasonally varying) sea-ice.

This is parameterized depending on the near-surface temperature of the appropriate grid cells. The surface albedo of the Antarctic continent depends on the ice and snow content of the corresponding grid cell and combines albedos of land (0.3), ice (0.35) and snow (0.75). A more detailed description of the climate forcing can be found in the appendix.

2.2 Climate sensitivity of the model

The equilibrium climate sensitivity as estimated from 19 atmospheric general circulation models ranges from 2.1 to 4.4°C, with an average of 3.2°C (Randall et al., 2007). These models do not include a dynamic ice-sheet component, but do account for changes in snow cover and albedo. The large spread in sensitivity is introduced by differences in feedback parameterizations. To tune the climate sensitivity of our model, we first ran the coupled ice sheet-climate model for the last 100 ka with constant pre-industrial pCO_2 of 280 ppm and varying orbital parameters. The modeled present-day ice sheet is in equilibrium with the radiative forcing and has a volume of 25.1×10^{15} m^3, similar to its estimated present-day size (e.g., Huybrechts et al., 2000; Oerlemans, 2002; Huybrechts, 2004). The mean hemispheric surface temperature is 14.8°C. The model is tuned such that a doubling of pCO_2 gives a reasonable temperature increase. We deliberately enhanced the sensitivity to changes in pCO_2 in order to account for the missing water vapor feedback (see Appendix). In the tuned model, a doubling of pCO_2 while maintaining fixed ice-sheet height and (seasonal) insolation distribution resulted in a hemispheric mean temperature increase of 2.8°C. This value falls well within the range of the values reported by the IPCC report (2007). The largest increase is found in atmospheric and surface temperatures in the Antarctic, high latitude box, with values up to 11.6°C. The large polar amplification is due to the included ice-albedo feedback.

CPD
4, 859–895, 2008

2.3 Insolation and pCO_2 forcing

Based on Earth's orbital elements as computed by Laskar et al. (2004) we compute daily insolation (Berger, 1978a,b) at the top of the atmosphere (for every latitude box) and at the surface for the high resolution Antarctic cells (60–90° S). We will use two different averages for comparison to ice-volume variations: annual mean and caloric summer (half-year of highest values) insolation. Since the atmospheric CO_2 level in the Middle Miocene is not very well constrained, the model is forced by prescribed scenarios of constant pCO_2, constant decrease in pCO_2 and a pCO_2 forcing including a 100-ka cycle (eccentricity).

2.4 Experimental set-up

First, hysteresis experiments are carried out, in order to find pCO_2-threshold values at which the Antarctic continent (de)glaciates. In addition, different levels of constant atmospheric CO_2 are applied for model runs of 1 Ma, from 14.2 to 13.2 Ma (preceded by a 100 k spin-up time), in order to investigate the effect of insolation fluctuations on ice-sheet volume under different constant pCO_2 conditions. Between 200 and 450 ppm, every 10 ppm is used for constant model forcing, with an increased resolution of 5 ppm between 390 and 410 ppm. Second, sensitivity experiments involving a reduction in pCO_2 are carried out, focusing on ice-sheet response to the level, speed and timing of pCO_2 decrease. Finally, pCO_2 forcing with a frequency of 100 ka is used to look into the mechanism causing eccentricity cycles within the sedimentary records. In all experiments specific daily insolation for appropriate latitudes is applied.

CPD
4, 859–895, 2008

3 Results

3.1 Hysteresis experiments

To assess the sensitivity of the simulated ice volume to pCO_2 changes and in order to find the critical range of pCO_2 at which the Antarctic continent (de)glaciates, two types of hysteresis experiments were performed. The first included orbital variations, while the second is only forced by atmospheric CO_2 (Fig. 2). In both experiments the (rapid) transition into a large ice-sheet occurred around 400 ppm, preceded by a semi-stable small ice sheet. In case of omitting orbital variations, deglaciation occurred at approximately 550 ppm, accounting for a hysteresis window of ~150 ppm. Orbital forcing acts as noise, therefore the ice sheet melts under much lower pCO_2 when it is included (~425 ppm). The modeled rate of pCO_2 change was slow at 50 ppm/Ma, comparable to the 280 ppm/5 Ma used by Pollard and DeConto (2005).

3.2 Constant pCO_2 experiments

The critical pCO_2 for glaciation is approximately 400 ppm. Below this threshold the entire Antarctic continent is glaciated, with mean ice volumes between 23 and 25×10^{15} m^3 (Fig. 3). Between ~405 and ~430 ppm (almost) continuous small ice sheets existed for the modeled period. Higher pCO_2 levels resulted in small, ephemeral ice sheets. Under constant pCO_2 forcing and insolation derived from orbital parameters of the Middle Miocene (between 14.2 and 13.2 Ma) either large or small ice sheets occurred (Figs. 3 and 4). Only constant pCO_2 values close to the threshold of 400 ppm caused a transition between these two states. Using constant 400 ppm forcing, Antarctic glaciated at 13.43 Ma. All small ice sheets showed large variations in ice volume, up to $\sim2.5\times10^{15}$ m^3 for constant pCO_2 of 410 ppm. Volume of large ice sheets varied less under constant pCO_2 conditions, with a maximum variance of $\sim1.1\times10^{15}$ m^3 for pCO_2 values close to the threshold and nearly no variance at lower pCO_2 levels. For further comparison two runs of constant pCO_2 close to the glaciation threshold value and with

CPD
4, 859–895, 2008

maximum ice-volume variance are used to represent the large ice sheet (390 ppm) and the small ice sheet (410 ppm).

The correlation between ice-volume variations and annual and summer mean insolation was computed for every 5° of southern latitude (Fig. 5). Both ice-sheet variations correlated better to high (around 70° S), than to low latitudes. In the case of the large ice-sheet, highest correlation coefficients were reached when ice volume lagged insolation by approximately 2 ka. Maximum correlation coefficient values were 0.29 and 0.75 for annual and summer mean, respectively. The small ice-sheet matched insolation averages best for a lag of 5 to 6 ka. Maxima for annual and summer mean insolation were 0.49 and 0.60, respectively.

3.3 Sensitivity experiments

In the first sensitivity experiment atmospheric CO_2 decreased linearly at a rate of 50 ppm/ka (Fig. 6 –red curves). For every experiment, the timing of the drop was simultaneous, only the extent, and therefore the initial and final levels of pCO_2 were different. The resulting ice volume transitions occurred around the same moment in time, whereby the largest difference in pCO_2 forced the most rapid ice-sheet transition (Fig. 6 – blue curves). This experiment focusing on initial and final levels of pCO_2 is repeated for different slopes of the pCO_2 transition, with identical results (not shown). The second test focused on the effect of the pace at which the atmospheric CO_2 is decreasing on the ice-sheet transition (Fig. 6). Experiments forced by a slow decrease in pCO_2 resulted in a variable duration of ice-sheet transition, between 20-30 ka. In runs with a fast pCO_2 drop, the transition length was independent of the speed of pCO_2 drawdown. This relation also holds for different timing of the pCO_2-transition (not shown). In the last sets of sensitivity experiments the forcing was applied at different moments in time (Fig. 7). Antarctica would have glaciated during the appropriate time interval (13.84–13.88 Ma) if a fast pCO_2 transition occurred around 13.9 Ma or due to a slower pCO_2 drawdown between 14.03 and 13.83 Ma.

4 Discussion

4.1 Constant pCO_2 experiments

In our coupled ice sheet-climate model, which is tuned to present-day conditions and a climate sensitivity of 2.8°C, relatively stable, large ice sheets occurred under pCO_2 below ~400 ppm (Fig. 3). Very stable ice sheets under relatively low pCO_2 levels (below 235 ppm) showed extremely small ice-volume variations. Correlations between continental ice volume and benthic oxygen isotopes vary between 1‰ (Zachos et al., 2001) and 2.2‰ (Pekar et al., 2002) for 100 m sea-level change. Taking the present ocean area (3.6×10^6 km^2) and the densities of water and ice (1000 kg/m^3 and 910 kg/m^3, respectively), an apparent sea level (ASL) drop of 100 m is equivalent to the build-up of ice with a volume of approximetely 33×10^{15} m^3. Using the maximum oxygen-isotope sea-level calibrations (~2.2‰ ≈33×10^{15} m^3), the standard deviation in the oxygen-isotope ratio derived from ice volume would be approximately 0.002‰ (Table 2) and resulting global sea-level fluctuations would be impossible to detect in the geological record. Larger variances are found in the modeled ice-volume record for a constant pCO_2 of 390 ppm (for a large ice sheet) and 410 ppm (for the small one) (Fig. 3). Ice-volume fluctuations in the small (big) ice sheet accounted for a maximum of 77% (41%) of the mean of the standard deviations in the benthic oxygen-isotope records (standard deviations are computed from the orginal oxygen-isotope data and afterwards averaged for comparison to the modeled ice-volume fluctuations; Tables 1 and 2). The modeled result that small ice sheets were more easily perturbed than large ice sheets can partly be traced back to the oxygen-isotope record (Table 1). An F-test showed that the variances of the original oxygen-isotope data in the restricted time domains were significantly different (significance level of 95%). This difference might be explained by the fact that small ice sheets are more easily perturbed by changes in the forcing. Additionally, ablation, which plays a major role in ice-volume variations, occurred on two sides of the small ice sheet, whereas the large ice sheet only had an ablation zone at the outer rim. Considering the very crude calibration used to compute these values, not

CPD
4, 859–895, 2008

taking care of any effects caused by changes in (deep sea) temperature, salinity, local runoff, oxygen-isotope ratio of the ice and so on, the correlation between the standard deviations of data- and model derived oxygen-isotope ratios is surprisingly high. Further more, these experiments were performed under constant pCO_2-levels. In the final part of this paper an experiment forced by large pCO_2 fluctuations will be discussed.

The synchronous minima of eccentricity and obliquity at ~13.84 Ma (Abels et al., 2005) result in a relatively constant and average-to-low insolation, which has been proposed as being partly responsible for the large-scale glaciation in the Middle Miocene (Holbourn et al., 2005). In our ice sheet-climate model, the occurrence of such a special configuration or the natural variability in insolation by itself is not sufficient for an Antarctic glaciation. Only constant atmospheric CO_2 levels at or very close to the threshold of 400 ppm induced a transition from small to large ice volume (Fig. 3), in a period that does not precisely corresponding to the transition depicted from oxygen isotope records. Therefore, in order to appropriately glaciate the Antarctic continent, some decrease in pCO_2 must have occurred.

4.2 Sensitivity experiments

In order to constrain the atmospheric CO_2 transition in the Middle Miocene, experiments with a constant pCO_2 decrease were performed. Three important factors defining the transition (the amount of pCO_2 drawdown, the slope and the timing of the event) are highly unknown, and were therefore tested in the following sensitivity experiments. First the ice-sheet model is forced by a decrease in atmospheric CO_2 with identical slopes and timing (Fig. 6 –red curves). The resulting glaciations occurred around the same time, with some difference in ice-sheet growth efficiency. The larger the difference between initial and final pCO_2, the faster the transition was. This can be explained by the different variability of the ice sheet at different pCO_2 levels. The larger standard deviations of 1.059×10^{15} m^3 and 2.542×10^{15} m^3 (Table 1) in the 390– and 410 ppm-runs, respectively, enhance the possibility for insolation variations to act against a rapid ice-volume transition. Because of the fact that sedimentary records

do not indicate such a rapid glaciation (e.g., Holbourn et al., 2005) and do show large variance in time, the relatively small difference in pCO_2 (410 to 390 ppm) is used for the remaining experiments.

The second sensitivity test dealt with the slope of the atmospheric CO_2 drawdown (Fig. 6 – blue curves). Six experiments with slopes varying between 20 ppm/2 ka to 20 ppm/200 ka were overlapping in time and had equivalent initial and final pCO_2 levels. For most runs, the ice-volume transition took place at the same moment. Exception was the slowest forcing (20 ppm/200 ka), which glaciates much later. The duration of the ice-sheet transition was defined as the period in which ice volume is larger than the maximum volume of the small ice sheet and smaller than the minimum size of the large ice sheet. Additional experiments show that slow forcing does not have a strong correlation to the time necessary for glaciation (not shown). It is also evident that the rate of pCO_2 drop has no effect on the length of the ice-sheet transition. The duration merely depends on the timing of the pCO_2 drop. This quite constrained timing (see next paragraph) limits the glaciation event to a length of approximately 30 ka. Compared to the duration of glaciation depicted by available data (30–40 ka according to $\delta^{18}O$ records by e.g. Holbourn et al., 2005) this is on the fast side, indicating that the ice-sheet model may respond more rapidly than the real Antarctic ice sheet. Most probably the difference in pCO_2 before and after the transition is relatively small, in the order of 100–200 ppm cf. Pearson and Palmer (2000); Royer et al. (2001); Pagani et al. (2005); Kürschner et al. (2008); Zachos et al. (2008), which make the slowest pCO_2 transitional experiments not very likely.

Nevertheless, the third set of sensitivity experiments investigated the timing of the pCO_2 decrease, for the (too) slow pace of 20 ppm/200 ka and for the faster and more realistic speed of 20 ppm/4 ka (Fig. 7). The best fit to data (glaciation time shown by vertical green lines) occurred either with a fast drawdown around 13.9 Ma, or a slow drawdown starting centered around 13.925–13.95 Ma (bold lines). Shifting this by only 2 ka resulted into a much earlier (~13.91 Ma) or later (~13.78 Ma) glaciation. This experiment was based on a 20 ppm difference in pCO_2, but extending this range would

give similar results (see first sensitivity test).

The comparison of the three sensitivity experiments to glaciation- and pCO_2-estimates from sedimentary records indicates that the pCO_2 drop should cross the threshold at approximately 400 ppm and should have occurred just before the ice-sheet transition (around 13.9 Ma) with a slope of approximately 20 ppm/4 ka (corresponding to ~150 ppm/30 ka). Because of the fact that the exact values are model dependent, these numbers should only be taken as guidelines, but they do put some constraints on the amount, pace and extent of the pCO_2-decrease.

Our results also contradict the hypothesis that Antarctic glaciation partly originated due to synchronous minima in eccentricity and obliquity around 13.84 Ma (e.g., Holbourn et al., 2005; Abels et al., 2005). The ice sheet-climate model is forced by daily insolation, which were averaged over the whole year (annual mean) and over the caloric summer (half year of largest daily insolation) to promote comparison to the resulting ice-volume variations. The two upper panels in Fig. 3 show the annual and summer mean insolation over the Middle Miocene period. The latitude of 70° S is chosen, because the large as well as the small ice-sheet volume variations correlated best to this latitude, although with a different lag time (see Result section). The combined minima in eccentricity and obliquity at ~13.84 Ma resulted in an average to high summer and annual mean insolation at 70° S. From the sensitivity experiments it can be seen that Antarctic glaciation is favored by maxima in ice-volume variations of the small ice sheet. These maxima are correlated to minima in insolation. For an ice-sheet extension in the Middle Miocene to occur, similar as illustrated by benthic oxygen-isotope records, the minima in high-latitude insolation at approximately 13.88 Ma is the most suitable candidate. So, instead of pointing to 13.84 Ma as an important insolation moment for the Antarctic glaciation, 13.88 Ma is more appropriate.

4.3 100-ka cycles

Without a carbon cycle implemented in the ice sheet-climate model, it is of course difficult to discuss possible interactions between the carbon cycle, ice volume and global

climate. On the other hand the low computation time allowed us to easily test the effect of various pCO_2 scenarios on ice volume. Here we focus on pCO_2-cycles with a frequency of 100 ka, similar to glacial-interglacial cycles of the Quaternary. It has been proposed that these cycles are caused by variability in the carbon cycle (e.g., Shackleton, 2000; Pälike et al., 2006) in contrast to studies showing that internal ice-sheet dynamics could result in the appropriate periodicity (Pollard, 1982, 1983). Following the previous ideas, the model was forced by atmospheric CO_2 changes that included a 100-ka cycle. Glacial-interglacial-like ice-volume cycles are found when the mean pCO_2 is around 420 ppm and the amplitude is about 40 ppm (Fig. 8). This is comparable to the ~50 ppm amplitude in pCO_2 found in ice-core records (e.g., Petit et al., 1999). When maxima in pCO_2 are close to maxima in eccentricity, the 100-ka cycle is most apparent. Similar to ice-volume cycles in the late Quaternary recorded in marine sediment records (e.g., Lisiecki and Raymo, 2005) the modelled ice volume showed slow ice build-up and rapid terminations. This asynchronous, threshold behaviour originates from internal model feedbacks, as the eccentricity rhythm within the input forcing was purely sinusoidal. Ice volume lagged pCO_2 with approximately 11–16 ka, which is in range with the 14 ka deducted by Shackleton (2000).

5 Conclusions

Despite the relatively simple geometry of our ice sheet-climate model, the realistically tuned climate sensitivity and hysteresis experiments indicate that the mechanism described in the following conclusions can be considered robust. However, exact numbers are model dependent and should only be taken as a guideline.

1. It is very unlikely that a constant pCO_2 forcing induced the large-scale Antarctic glaciation in the Middle Miocene. Constant levels produced either a large (below ~400 ppm threshold) or a small (above ~400 ppm) ice sheet. Large ice sheets covered the whole Antarctic continent and had a smaller ice-volume variation than

expected from sedimentary deep-sea records (~41%). The variance in the small ice sheet explained the fluctuation in oxygen-isotope ratios in these records for ~78%. Residual variation in the isotope records can originate from fluctuations in pCO_2 or other changes in climatic conditions. Ice-volume variations correlated best to insolation at relatively high latitudes (~70° S). In case of the small ice sheet summer mean insolation was the main forcing, which lead ice volume by ~2 ka. Ice volume lagged insolation by 5-6 ka in the large ice sheet and correlated only to some extent better to summer than annual mean values.

2. The extent of the pCO_2 drawdown was not important for timing or duration of the glaciation event, as long as it crosses the 400 ppm threshold. Moderate or quick pCO_2 reductions resulted in comparable and realistic ice-sheet extension. The ice-sheet response was fast, which limited the pCO_2 drawdown to happen around 13.9 Ma. A relatively slow drop in pCO_2 caused a delayed glaciation and had to occur at 13.925–13.950 Ma. The best guess for the Middle Miocene pCO_2 decline was a scenario crossing the threshold of 400 ppm around 13.9 Ma with a speed of approximately 150 ppm/30 ka.

3. Forcing the ice sheet-climate model with 100-ka pCO_2 cycles of 40 ppm amplitude resulted in late Pleistocene ice-age-like behavior, with slow ice-volume build-up, and rapid terminations. Ice-volume variations lagged pCO_2 cycles by 11–16 ka, similar to what had been found by Shackleton (2000).

Appendix A

Model description

The ice sheet-climate model is controlled by energy and mass balances. Orbital elements are derived following the work of Laskar et al. (2004). They drive the seasonal

solar radiation at the top of the atmosphere and define, together with the pCO_2, the amount of energy entering the entire climate system.

A1 Energy and temperature balances

The model consists of three large-scale boxes covering the entire southern hemisphere: a low (0–30° S), middle (30–60° S) and high (60–90° S) latitude box (Fig. 1). Within the climate system energy is conserved and changes in time are described by (Pollard, 1983; Hartmann, 1994):

$$\frac{\partial E_{ao}}{\partial t} = R_{TOA} + \Delta F_{ao} + LH \tag{A1}$$

where E_{ao} is the total energy in the system, t the time of year, R_{TOA} the net incoming solar radiation on the top of the atmosphere, ΔF_{ao} the divergence of the meridional energy transport in the ocean as well as in the atmosphere, and LH the latent heat added to the atmosphere after condensation and freezing of water vapor. The net incoming radiation is the sum of the incoming short-wave radiation (SW_p) and the outgoing short- and long-wave radiation (LW_p):

$$R_{TOA} = SW_p^{\downarrow} - SW_p^{\uparrow} - LW_p^{\uparrow}.$$

Radiation fluxes in the two *lower latitude* boxes (0–30° S and 30–60° S) are parameterized as:

$$SW_p^{\downarrow} - SW_p^{\uparrow} = Q(1 - \alpha_p)$$

$$LW_p^{\uparrow} = \varepsilon_p \sigma T_a^4 + f_{CO_2}$$

where Q is the solar insolation at the top of the atmosphere, α_p the planetary albedo, ε_p the planetary emissivity and σ the Stefan-Boltzmann constant. T_a is interpreted as

CPD
4, 859–895, 2008


the near-surface air temperature and f_{CO_2} as the effect of the atmospheric CO_2 content (cf., Myhre et al., 1998):

$$f_{CO_2} = -4\frac{\ln(\frac{CO_2}{280})}{\ln(2)} \approx 2.8 - 0.7\ln(CO_2).$$

Therefore, a doubling of pCO_2 from 280 ppm (pre-industrial conditions) to 560 ppm accounts for a reduction of 4 W/m^2 in the outgoing longwave radiation of the two lower latitude boxes.

The physical processes in the *high latitude* box are deciphered in much higher resolution and complexity. For every 0.5° latitude energy and mass balances for the atmosphere and for the surfaces are simultaneously solved. Atmospheric temperature (T_a) is described by:

$$C_a\frac{dT_a}{dt} = R_a + LW + SH + LH_{\text{eva}} + LH_{\text{snow}}$$

and surface temperature (T_s) by:

$$C_s\frac{dT_s}{dt} = R_s - LW - SH - LH_{\text{eva}} - F_s - F_m$$

where $C_{a,s}$ is the heat capacity for the atmosphere and surface, respectively.

The incoming energy at the top of the atmosphere and at the surface is represented as (Jentsch, 1987; Wang and Mysak, 2000):

$$\begin{aligned} R_a &= SW_a^{\downarrow} - SW_a^{\uparrow} - LW_a^{\uparrow} \\ &= Q(1-\alpha_a)(1-\tau)(1+\tau\alpha_s) - (\varepsilon_2\sigma T_a^4 + (1-\varepsilon_1)\sigma T_s^4) \end{aligned}$$

$$\begin{aligned} R_s &= SW_s^{\downarrow} - SW_s^{\uparrow} \\ &= \tau Q(1-\alpha_a)(1-\alpha_s) \end{aligned}$$

where τ is the atmospheric transmissivity of solar radiation, $\alpha_{a,s}$ the atmospheric and surface albedos, ε_2 an emissivity constant and ε_1 a term describing the greenhouse effect (see below).

The longwave and sensible heat fluxes between the atmosphere and surface are parameterized as:

$$LW = \sigma T_s^4 - \varepsilon_1 \sigma T_a^4$$

$$SH = \lambda(T_s - T_a)$$

where λ is a heat exchange coefficient which in principle depends on wind speed, atmospheric density and heat capacity, but is taken to be constant. The heat flux into the subsurface soil or upper ice layer (F_s) is given by:

$$F_s = \frac{2k_1}{\Delta z_1}(T_s - T_a)$$

where k_1 is the thermal conductance of snow and Δz_1 the depth range of conduction.

The latent heat of evaporation (LH_{eva}) is parameterized as (Hartmann, 1994):

$$LH_{\text{eva}} = \rho_{\text{air}} L_v C_{\text{DE}} U[q_s^*(1 - RH) + \frac{RH}{B_e}\frac{c_p}{L_v}(T_s - T_a)]$$

where ρ_{air} is the air density, L_v is the latent heat of vaporation, C_{DE} an exchange coefficient, U the wind speed, q_s^* the sea surface humidity, B_e the equilibrium Bowen ratio, c_p the specific heat of dry air and RH the relative humidity.

The latent heat associated with snowfall (LH_{snow}) depends on the accumulation of snow:

$$LH_{\text{snow}} = L_s A$$

where L_s is the latent heat of sublimation and A the accumulation. The snow is considered to be evaporated in the low latitude box, accounting for the LH-term in the energy equation (Eq. **??**). The total accumulation and its latitudinal distribution is tuned to the present-day total Antarctic accumulation and depends on the distance to the South Pole (r), the surface height (h_{sfc}) and the daily surface temperature (T_s) (Oerlemans, 2002, 2004). It therefore includes processes such as the elevation-desert effect (Pollard, 1983):

$$A = (c_a + c_b r) e^{\frac{-h_{\mathrm{sfc}}(r)}{c_d}} e^{\kappa T_s}$$

where $c_{a,b}$ are (tuning) constants, c_d is a characteristic length scale and κ a constant describing the precipitation dependence on temperature. Only when the local temperature is below 2°C, snow is accumulated (Oerlemans, 2001).

The amount of energy available for melting (F_m) depends on the incoming energy and the thickness and heat capacity of the top layer (Fraedrich et al., 2005). The affected layer is 20 cm deep (d_{top}) and consists of snow (d_{snow}), soil (d_{soil}) or a mixture of both. The heat capacity (C_s) used for computation of the surface temperature is therefore computed by:

$$C_s = \frac{C_{\mathrm{snow}} C_{\mathrm{soil}} d_{\mathrm{top}}}{C_{\mathrm{snow}} d_{\mathrm{soil}} + C_{\mathrm{soil}} d_{\mathrm{snow}}}$$

The atmospheric and surface temperature equations are simultaneously solved. Daily computation is necessary, because the orbital cycle as well as processes of snow accumulation and melting have a strong seasonal imprint (Pollard, 1983). The meridional heat transport (ΔF_{eo}) accounts for the coupling between the boxes, and is proportional to the temperature gradient based on the diffusion approximation (Sellers, 1970; North, 1975). The atmospheric temperatures, and also the surface temperatures, are further extrapolated towards their altitudes (h_{sfc}) according to the prescribed lapse rate, Γ_{lapse}:

$$T_a = T_a + \Gamma_{\mathrm{lapse}} h_{\mathrm{sfc}}(r).$$

A2 Mass balance

The mass balance is solved cumulatively on a daily basis. The specific mass balance, the total amount of accumulation or ablation (per latitude) within one year, possibly reduced by (surface or bottom) melting, evaporation or calving, is annually added to or subtracted from the snow/ice-sheet.

The ice sheet is allowed to grow into the surrounding ocean as long as it is hydrostatically floating. When the total weight of the ice column exceeds the floating criteria, calving occurs (Pollard, 1982) and the total mass balance (G) will be set to a negative value (c_{bal}):

$$G = c_{\mathrm{bal}} \text{ if } \rho_{\mathrm{air}} h_{\mathrm{ice}} < \rho_w (h_{\mathrm{sfc}} - h_{\mathrm{ice}})$$

where ρ_{ice} and ρ_w are the densities of ice and water, respectively, h_{ice} is the ice thickness, and h_{sfc}, the elevation of the surface with respect to the current sea level, which is taken as a constant reference level. This crude calving parameterization also accounts for occurrence of proglacial lakes and/or marine incursions (Pollard, 1982).

Bottom melting (S) occurs when the temperature in the basal layer (T_{base}) exceeds the pressure melting point (T_{pmp}):

$$S = \frac{C_{\mathrm{ice}}}{L_m}(T_{\mathrm{base}} - T_{\mathrm{pmp}})\frac{\Delta z_{\mathrm{base}}}{\Delta t}$$

where C_{ice} is the specific heat of ice and L_m the specific latent heat of fusion of ice and Δz_{base} the thickness of the basal layer.

A3 Albedo

A separate snow balance is computed to parameterize the surface albedo. The formulas for this cumulative balance resemble the previous surface mass and energy balance

equations, except for the fact that the snow depth cannot become negative. The daily derived surface albedo (α_s) depends on the snow depth (d_{snow}), when the snow layer is thicker than 10 cm:

$$\alpha = \frac{\alpha_{\text{snow}} + \alpha_{\text{ice}}}{2} + \frac{\alpha_{\text{snow}} - \alpha_{\text{ice}}}{2} \tanh(A_{\text{snow}}(d_{\text{snow}} - B_{\text{snow}}))$$

where the slope (A_{snow}) and shift (A_{snow}) are constant and α_{snow} and α_{ice} are the albedos of snow and ice, respectively. When there is less or no ice/snow, the land, ocean (low and middle latitude boxes) or sea-ice albedos (high latitude box) are used. The latitudinal extent of sea-ice (lat_{si}) is given by (Jentsch, 1987):

$$lat_{\text{si}} = \sin^{-1}[\tanh(x_0(\frac{T_{\text{pd}}}{T_a})^{x_1})] - C_{\text{si}}$$

where x_0 and x_1 are tuning constants, T_{pd} a measure for the present-day value of sea-water temperature and C_{si} a latitudinal shift.

The planetary (α_p) and atmospheric (α_a) albedos are parameterized as functions of latitude (Wang and Mysak, 2000):

$$\alpha_p = 0.6 - 0.4\cos(\text{lat})$$

$$\alpha_a = 0.3 - 0.1\sin(\text{lat}).$$

A4 Greenhouse effect

The longwave radiation constant ε_1 accounts for the greenhouse effect due to $p\text{CO}_2$ and other greenhouse gases:

$$\varepsilon_1 = \varepsilon_{10} + \varepsilon_{11}\sqrt{e'}$$

where, e' is the atmospheric vapor pressure, related to the saturation specific humidity (q_{sat}) and relative humidity (RH):

$$e' = 1.6 \times 10^3 \mathrm{RH} q_{sat}$$

where:

$$q_{sat} = \frac{1.57 \times 10^{11}}{\rho_{air} R_{air} T_a} e^{\frac{-5421}{T_a}}$$

with R_{air} being the gas constant for dry air.

According to Staley and Jurica (1970) and Jentsch (1991), the CO_2-emission factor can be parameterized by:

$$\varepsilon_{10}^{CO_2} = 0.1 + 0.025 \ln(CO_2). \quad \text{(A2)}$$

The other main greenhouse gas, water vapor (H_2O), also contributes about half to the (present-day) greenhouse effect. Because of the fact that we do not explicitly compute the hydrological cycle, this feedback can not be parameterized separately. To still include the effect of water vapor, we increased the climate sensitivity to pCO_2 Eq. A2 is therefore expanded and retuned to:

$$\varepsilon_{10} = \varepsilon_{10}^{CO_2} + \varepsilon_{10}^{H_2O} = 0.1 + 0.025 \ln(CO_2).$$

A doubling of atmospheric CO_2 now results in a climate sensitivity of 2.8°C and modeled present-day ice-sheet size, accumulation and temperature distribution are similar to estimates (Huybrechts et al., 2000; Oerlemans, 2002).

A5 List of constant parameters

Table A5 gives an overview of the parameters used in the ice sheet-climate model.

Acknowledgements. This project was funded by the DFG (Deutsche Forschungsgemeinschaft) within the European Graduate College "Proxies in Earth History".

References

Abels, H., Hilgen, F., Krijgsman, W., Kruk, R., Raffi, I., Turco, E., and Zachariasse, W.: Long-period orbital control on middle Miocene global cooling: Integrated statigraphy and astronomical tuning of the Blue Clay Formation on Malta, Paleoceanography, 20, 2362–2367, doi:10.1029/2004PA001129, 2005. 868, 870

Berger, A. L.: Long Term Variations of Caloric Insolation resulting from the Earth's orbital elements, Quat. Res., 9, 139–167, 1978a. 864

Berger, A. L.: Long Term Variations of Daily Insolation and Quaternary Climatic Changes, J. Atmos. Sci., 35, 2362–2367, 1978b. 864

Coxall, H., Wilson, P., Pälike, H., Lear, C., and Backman, J.: Rapid stepwise onset of Antarctic glaciation and deeper calcite compensation in the Pacific Ocean, Nature, 443, 53–57, 2005. 861

Flower, B. and Kennett, J.: Middle Miocene deep-water paleoceanography in the Southwest Pacific relations with East Antarctic ice-sheet development, Paleoceanography, 10, 1095–1112, 1995. 861

Fraedrich, K., Jansen, H., Kirk, E., and Lunkeit, F.: The Planet Simulator: towards a user friendly model, Meteor. Zeitschrift, 14, 299–30, 2005. 876

Hartmann, D. L.: Global Physical Climatology, Academic Press, San Diego, 1994. 873, 875

Holbourn, A., Kuhnt, W., Schulz, M., and Erlenkeuser, H.: Impacts of orbital forcing and atmospheric carbon dioxide on Miocene ice-sheet expansion, Nature, 438, 483–487, 2005. 860, 861, 868, 869, 870, 884

Holbourn, A., Kuhnt, W., Schulz, M., Flores, J.-A., and Anderson, N.: Orbitally-paced climate evolution during the middle Miocene Monterey carbon-isotope excursion, Earth Planet. Sci. Lett., 261, 534–550, 2007. 861

Huybrechts, P.: Antarctica, in: Mass balance of the cryosphere: observations and modelling of contemporary and future changes, edited by J.L., B. and Payne, A., 491–523, Cambridge University Press, Cambridge, United Kingdom, 2004. 863

Huybrechts, P., Steinhage, D., Wilhems, F., and Bamber, J.: Balance velocities and measured properties of the Antarctic ice sheet from a new compilation of gridded data for modeling, Ann. Glaciol., 30, 52–60, 2000. 863, 879

Jentsch, V.: Cloud-ice-vapor feedbacks in a global climate model, in: Irreversible Phenomena and Dynamical Systems Analysis in Geosciences, edited by Nicolis, C. and Nicolis, G.,

Reidel Publishing Company, Dordrecht, The Netherlands, 1987. 862, 874, 878, 886
Jentsch, V.: An Energy Balance Climate Model With Hydrological Cycle. 1. Model Description and Sensitivity to Internal Parameters, J. Geophys. Res., 96, 17 169–17 179, 1991. 862, 879
Kürschner, W., Kvacek, Z., and Dilcher, D.: The impact of Miocene atmospheric carbon dioxide fluctuations on climate and the evolution of terrestrial ecosystems, Proc. Nat. Acad. Sci. USA, 106, 449–453, 2008. 861, 869
Laskar, J., Robutel, P., Joutel, F., Gastineau, M., Correia, A., and Levrard, B.: A long-term numerical solution for the insolation quantities of the Earth, Astron. & Astrophys., 428, 261–285, 2004. 862, 864, 872
Lisiecki, L. and Raymo, M.: A Plio-Pleistocene stack of 57 globally distributed benthic $\delta^{18}O$ records, Paleoceanography, 20, 522–533, doi:10.1029/2004PA001071, 2005. 871
Lythe, M., Vaughan, D., and the BEDMAP Consortium: BEDMAP - bed topography of the Antarctic. 1:10 000 000 scale map, British Antarctic Survey, Cambridge, United Kingdom, 2000. 862
Miller, K., Mountain, G., Browning, J., Kominz, M., Sugarman, P., Christie-Blick, N., Katz, M., and Wright, J.: Cenozoic global sea level, sequences, and the New Jersey transect: results from coastal plan and continental slope drilling, Rev. Geophys., 36, 569–601, 1998. 861
Miller, K., Kominz, M., Browning, J., Wright, J., Mountain, G., Katz, M., Sugarman, P., Cramer, B., Christie-Blick, N., and Pekar, S.: The Phanerozoic record of global sea-level change, Science, 310, 1293–1298, 2005. 861
Myhre, G., Highwood, E., Shine, K., and Stordal, F.: New estimates of radiative forcing due to well mixed greenhouse gases, Geophys. Res. Lett., 25, 2715–2718, 1998. 874
North, G. R.: Theory of Energy Balance Climate Models, J. Atmos. Sci., 32, 2033–2043, 1975. 876
Oerlemans, J.: Glaciers and climate change, in: Modeling glacier mass balance, edited by Oerlemans, J., chap. 4, Balkema, The Netherlands, 2001. 876
Oerlemans, J.: Global dynamics of the Antarctic ice sheet, Clim. Dynam., 19, 85–93, 2002. 862, 863, 876, 879
Oerlemans, J.: Antarctic ice volume and deep-sea temperature during the last 50 Myr: a model study, Ann. Glaciol., 39, 13–19, 2004. 862, 876
Pagani, M., Zachos, J., K.H., F., Tipple, B., and Bohaty, S.: Marked decline in atmospheric carbon dioxide concentrations during the Paleogene, Science, 309, 600–603, 2005. 861, 869

Pälike, H., Norris, R., Herrle, J., Wilson, P., Coxall, H., Lear, C., Shackleton, N., Tripati, A., and Wade, B.: The heartbeat of the Oligocene Climate System, Science, 314, 1894–1898, 2006. 871
Pearson, P. and Palmer, M.: Atmospheric carbon dioxide concentrations over the past 60 million years, Nature, 406, 695–699, 2000. 861, 869
Pekar, S., Christie-Blick, N., Kominz, M., and Miller, K.: Atmospheric carbon dioxide concentrations over the past 60 million years, Geology, 30, 903–906, 2002. 867, 885
Petit, J., Jouzel., J., Raynaud, D., Barkov, N., Barnola, J.-M., Basile, I., Bender, M., Chappellaz, J., Davis, M., Delaygue, G., Delmotte, M., Kotlyakov, V., Legrand, M., Lipenkov, V., Lorius, C., Pépin, L., Ritz, C., Saltzman, E., and Stievenard, M.: Climate and atmospheric history of the past 420,000 years from the Vostok ice core, Nature, 399, 429–436, 1999. 871
Pollard, D.: A simple ice sheet model yields realistic 100 kyr glacial cycles, Nature, 296, 334–338, 1982. 862, 871, 877
Pollard, D.: A Coupled Climate-Ice Sheet Model Applied to the Quaternary Ice Ages, J. Geophys. Res., 88, 7705–7718, 1983. 862, 871, 873, 876
Pollard, D. and DeConto, R.: Hysteresis in Cenozoic Antarctic ice-sheet variations, Glob. Planet. Change, 45, 9–21, 2005. 861, 865, 889
Randall, D., Wood, R., Bony, S., Colman, R., Fichefet, T., Fyfe, J., Kattsov, V., Pitman, A., Shukla, J., Srinivasan, J., Stouffer, R., Sumi, A., and Taylor, K.: in: Climate Change 2007: The Scientific Basis. Contribution of Working Group 1 to the Fourth Assessment Report of the Intergovernmental Panel on Climate Change, edited by Solomon, S., Qin, D., Manning, M., Chen, Z., Marquis, M., Averyt, K., Tignor, M., and Miller, H., p. 881, Cambridge University Press, Cambridge, United Kingdom and New York, NY, USA, 2007. 863
Raymo, M. E.: The initiation of northern hemisphere glaciation, Paleoceanography, 9, 399–404, 1994. 861
Royer, D., Wing, S., Beerling, D., Jolley, D., Koch, P., Hickey, L., and Berner, R.: Paleobotanical evidence for near present-day levels of atmospheric CO_2 during part of the Tertiary, Science, 292, 2310–2313, 2001. 861, 869
Sellers, W. D.: A global climate model based on the energy balance of the earth-atmosphere system, J. Appl. Meteorol., 8, 392–400, 1970. 876, 886
Shackleton, N. J.: The 100,000-year ice-age cycle identified and found to lag temperature, carbon dioxide, and orbital eccentricity, Science, 289, 1897–1902, 2000. 871, 872
Shevenell, A., Kenneth, J., and Lea, D.: Middle Miocene Southern Ocean cooling and Antarctic

cryosphere expansion, Science, 305, 1766–1770, 2004. 861
Sima, A.: Modeling oxygen isotopes in ice sheets linked to Quaternary ice-volume variations, Ph.D. thesis, University of Bremen, Germany, 2005. 862
Sima, A., Paul, A., Schulz, M., and Oerlemans, J.: Modeling the oxygen-isotope composition of the North American Ice Sheet and its effect on the isotopic composition of the ocean during the last glacial cycle, Geophys. Res. Lett., 33, doi:10.1029/2006GL026923, 2006. 862
Staley, D. O. and Jurica, G. M.: Flux emissivity tablesfor water vapor carbon dioxide and ozone, J. Appl. Meteorol., 9, 365–372, 1970. 879
Wang, Z. and Mysak, L.: A simple coupled atmosphere-ocean-sea ice-land surface model for climate and paleoclimate studies, J. Climate, 13, 1150–1172, 2000. 862, 874, 878, 886
Zachos, J., Dickens, G., and Zeebe, R.: An early Cenozoic perspective on greenhouse warming and carbon-cycle dynamics, Nature, 451, 279–283, 2008. 861, 869
Zachos, J. C., Pagani, M., Sloan, L., Thomas, E., and Billups, K.: Trends, Rythms, and Aberrations in Global Climate 65 Ma to Present, Science, 292, 686–693, 2001. 860, 861, 867, 885

Table 1. Standard deviation of benthic oxygen-isotope records (‰) of Holbourn et al. (2005).

Time interval	(Ma)	References and comments
13.2–13.8	13.9–14.5	
0.160	0.207	Site 1146
0.127	0.159	Site 1237
0.144	0.183	Mean of above two standard deviations for comparison to modeled ice-volume fluctuations
(Fig. 4 left)	(Fig. 4 right)	

CPD
4, 859–895, 2008

Table 2. Standard deviation of modeled ice-volume variation and equivalent oxygen-isotope ratios using 33×10^{15} m^3=1‰ (Zachos et al., 2001) and 33×10^{15} m^3=2.2‰ (Pekar et al., 2002).

Time interval (Ma)	pCO_2 (ppm)	Standard deviation (10^{15} m^3)	ASL (m)	$\delta^{18}O$ (‰) (33×10^{15} m^3=1‰)	$\delta^{18}O$ (‰) (33×10^{15} m^3=2.2‰)	Percentage of data (%)
13.2–13.8	220	0.041	0.104	0.001	0.002	1% of 0.144
13.2–13.8	390	1.059	2.677	0.027	0.059	41% of 0.144
13.9–14.5	410	2.542	6.426	0.064	0.141	77% of 0.183

Table A1. List and desciption of constant parameters.

Symbol	Description	Value	Unit
ε_p	Planetary emissivity	0.61 (15° S)	–
		0.66 (45° S)	–
		0.69 (75° S)	–
ε_{11}	Emissivity constant (Sellers, 1970)	0.05	–
ε_2	Emissivity constant (Jentsch, 1987)	0.30	–
σ	Stefan-Boltzmann constant	5.67×10^{-8}	W m^{-2} K^{-4}
τ	Atmospheric transmissivity (Wang and Mysak, 2000)	0.65	–
λ	Heat exchange coefficient	10.0	W m^{-2} K^{-1}
k_1	Thermal conductance of snow	0.31	W m^{-1} K^{-1}
Δz_1	Depth range of subsurface conduction	3.0	m
ρ_{air}	Density of air	1.2	kg m^{-3}
ρ_{ice}	Density of ice	910	kg m^{-3}
ρ_w	Density of water	1000	kg m^{-3}
C_{DE}	Exchange coefficient for latent heat	1.0×10^{-3}	–
U	Wind speed	5.0	m s^{-1}
q_s^*	Sea surface specific humidity	0.8×10^{-3}	kg kg^{-1}
RH	Relative humidity (Bintanja, 1999, p. 122)	0.75	–
B_e	Equilibrium Bowen ratio	2.0	–
R_{air}	Gas constant for dry air	287.04	J kg^{-1} K^{-1} yr^{-1}
Γ_{lapse}	Atmospheric temperature lapse rate (Payne and Dongelmans, 1997)	–0.012	C m^{-1}
L_v	Latent heat of vaporation of ice	2.26×10^6	J kg^{-1}
L_m	Latent heat of melting of ice	0.334×10^6	J kg^{-1}
C_p	Specific heat capacity of dry air	1005	J kg^{-1}K^{-1}
C_{ice}	Specific heat capacity of ice	2009	J kg^{-1} K^{-1}

CPD
4, 859–895, 2008

Table A1. Continued.

Symbol	Description	Value	Unit
d_{top}	Affected snow/soil layer	0.2	m
c_d	Precipitation constant	3000.0	m
κ	Precipitation dependence on temperature	0.0345	K^{-1}
A_{snow}	Tangent hyperbolicus constant	50	–
B_{snow}	Tangent hyperbolicus constant	0.05	–
c_{bal}	Calving constant	–2	m yr^{-1}
α_{snow}	Albedo of snow	0.75	–
α_{ice}	Albedo of ice	0.35	–
α_{seaice}	Albedo of seaice	0.60	–
α_{land}	Albedo of land	0.30	–
α_w	Albedo of ocean water	0.10	–
x_0	Constant for sea-ice extent	2.1	–
x_1	Constant for sea-ice extent	0.6	–
T_{pd}	Temperature constant for sea-ice extent	–41	°C
C_{si}	Latitudinal shift constant for sea-ice extent	19	°

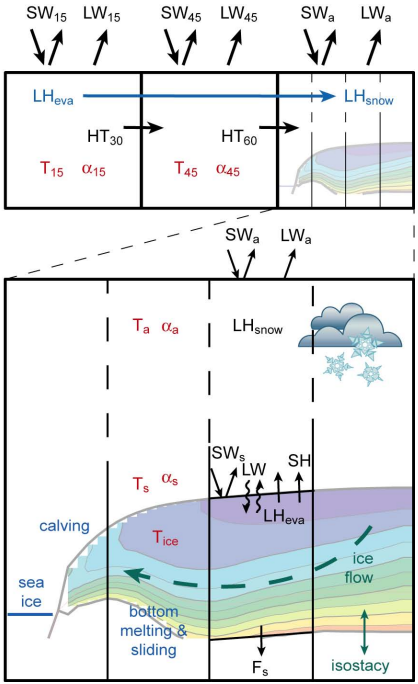

Fig. 1. Set-up of the model. Upper: Large-scale box model consisting of low (0–30°C S), middle (30–60°C S) and high (60–90°C S) latitude cells. Each compartment is forced by shortwave (SW) and longwave (LW) radiation at the top of the atmosphere and sensible heat transport by eddies (HT), as well as latent heat transport induced by evaporation and snowfall (LH). The two lower latitude boxes are described by one general temperature (T) and albedo (α). **Lower:** The high-latitude, Antarctic box is subdivided into smaller grid cells with a resolution of 0.5°C latitude. For each cell the energy and mass balances are solved for surface and atmospheric temperatures (T_s and T_a, respectively). Fluxes include incoming and outgoing shortwave radiation at the top of atmosphere (SW_a) and at the land/ice/snow surface (SW_s); reflected longwave radiation at the top of atmosphere (LW_a); longwave (LW), sensible heat (SH) and latent heat of evaporation (LH_{eva}) fluxes between the surface and atmosphere; latent heat of snowfall in atmosphere (LH_{snow}); heat flux into underlying bedrock (F_s). In all boxes ice flow velocities and ice height are computed, depending on the mass balance, local temperature (T), albedo (α) and isostasy.

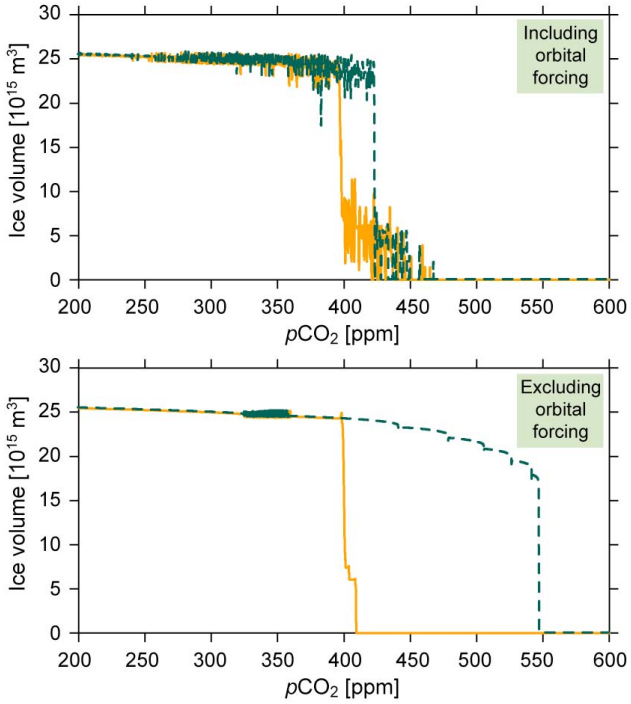

Fig. 2. Hysteresis experiment. Starting from no-ice conditions and high pCO_2 (orange solid) or starting from full ice sheet and low pCO_2 (green dashed). Upper panel shows hysteresis including orbital forcing, lower panel without orbital variations. Rate of pCO_2 change is 250 ppm/5 Myr, comparable to 280 ppm/5 Myr used by Pollard and DeConto (2005).

CPD
4, 859–895, 2008

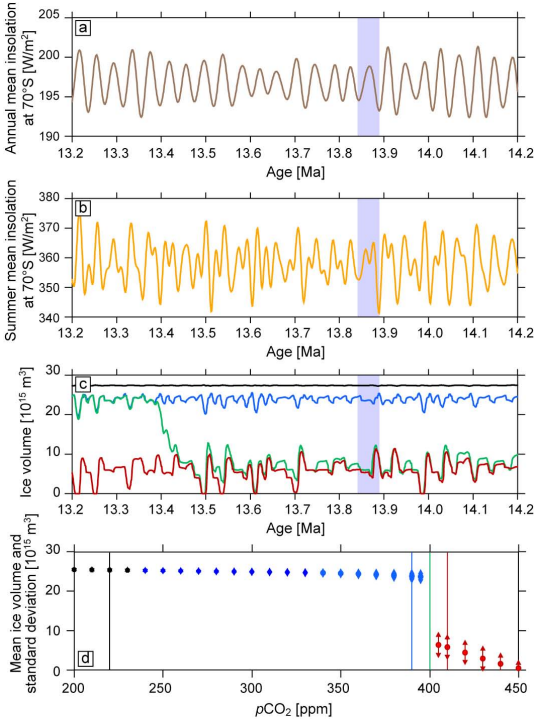

Fig. 3. Constant pCO_2 experiments in the Middle Miocene (14.2–13.2 Ma). **(a)** Annual mean insolation at 70° S. **(b)** Summer mean insolation at 70° S. **(c)** Resulting ice-volume variations of four typical pCO_2 forcing (220 ppm (black), 390 ppm (blue), 400 ppm (green) and 410 ppm (red). **(d)** Mean ice volume (dot) and standard deviation (arrows) of large (black/blue) and small (red) ice sheets, defined by their pCO_2 level. The blue rectangle encompasses the Middle Miocene glaciation period as depicted by oxygen isotope records.

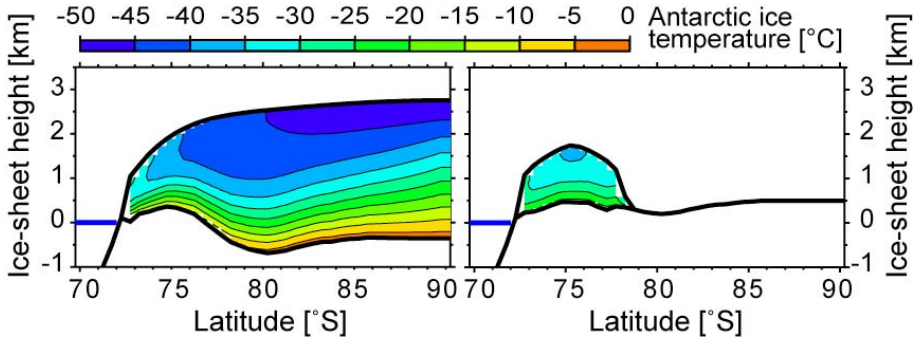

Fig. 4. Cross-section of large (left) and small (right) Antarctic ice sheets. Color scale corresponds to annual mean ice temperatures.

CPD
4, 859–895, 2008

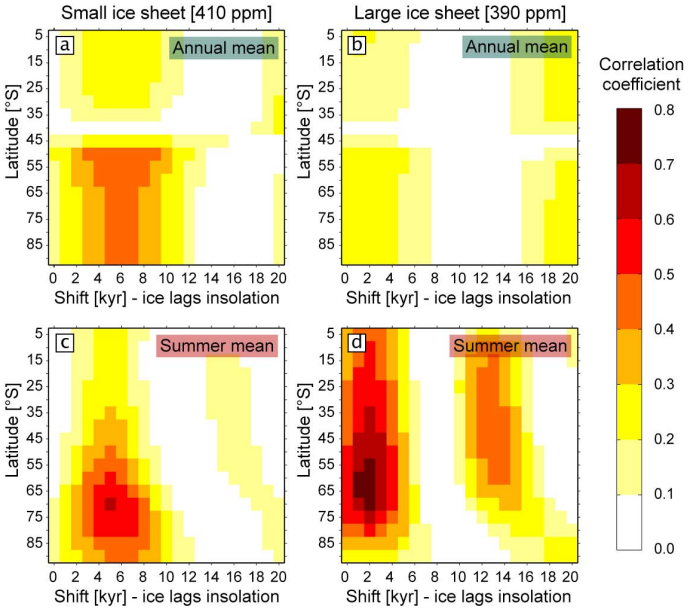

Fig. 5. Ice-sheet variations correlated to insolation at latitudes between 0 and 90° S. Insolation is shifted backwards per 1 ka on horizontal axis (ice volume lags insolation). Correlation coefficients are given for a small (**a** and **c**) and large (**b** and **d**) ice sheet and for annual (**a** and **b**) and summer mean (**c** and **d**) insolation. Best correlation is found for latitudes around 70° S and a shift of 5-6 ka (small ice sheet) or 2 ka (large ice sheet). Highest correlation coefficients for a small ice sheet are 0.49 and 0.60, for annual and summer mean insolation respectively. Maxima for a large ice sheet are 0.29 (annual) and 0.75 (summer mean insolation).

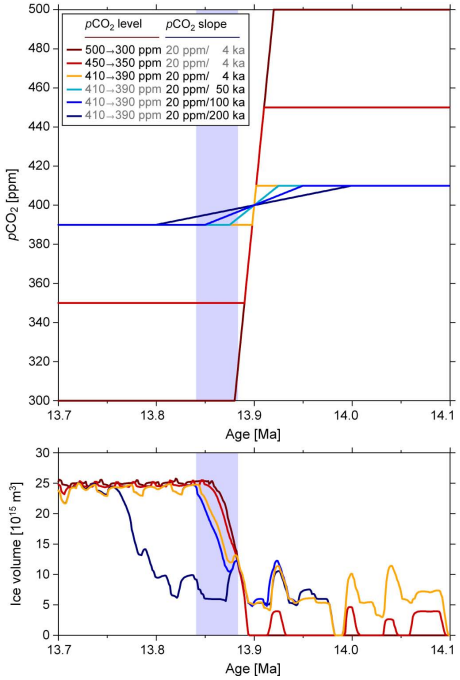

Fig. 6. pCO_2 sensitivity experiments – level of initial and final pCO_2 (red colors) and speed of pCO_2 decrease (blue colors). Colors in upper panel show pCO_2 forcing and correspond to ice-volume transition in lower panel. Blue box indicates approximate Antarctic glaciation as retrieved from sedimentary records. Glaciation is independent from initial and final pCO_2 levels (red to orange). On the contrary, the speed of the pCO_2 drawdown is important. Extremely slow drop in pCO_2 (dark blue) results in delayed ice-sheet extension, relatively slow decrease (light blue) causes appropriate timing with glaciation. A pCO_2 drop of 20 ppm/50 ka or faster (for example 20 ppm/4 ka in orange) give the same ice-sheet transition as 20 ppm/50 ka.

CPD
4, 859–895, 2008

Title Page
Abstract Introduction
Conclusions References
Tables Figures
◀I ▶I
◀ ▶
Back Close
Full Screen / Esc
Printer-friendly Version
Interactive Discussion

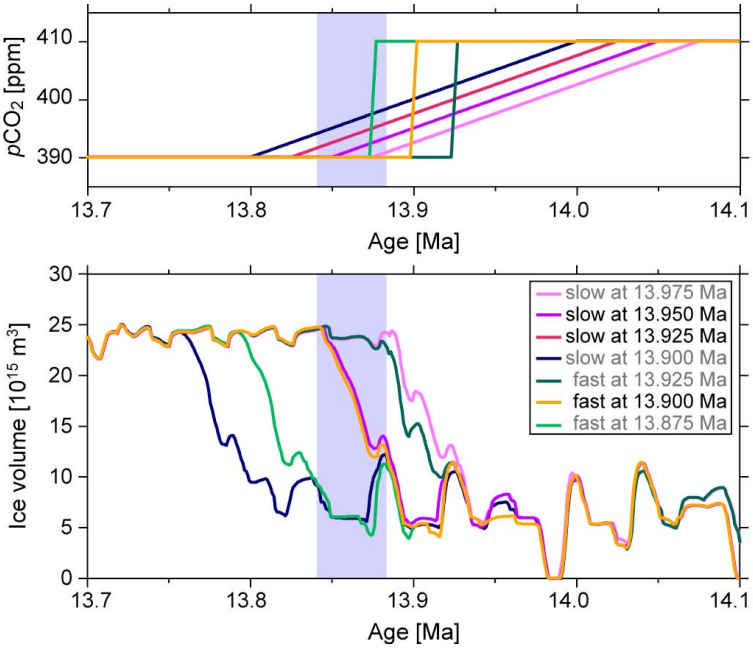

Fig. 7. pCO_2 sensitivity experiment – timing of pCO_2 decrease. Colors in upper panel show pCO_2 forcing and correspond to ice-volume transition in lower panels. Blue box indicates approximate Antarctic glaciation as found in sedimentary records. Green/orange curves result from fast pCO_2 transition (20 ppm/4 ka); purple/blue ones from a slow drop (20 ppm/200 ka). The center lines (black text in legend) indicate best fitting solutions (see Discussion section). Orange and dark blue curves correspond to their counterparts in Fig. 6.

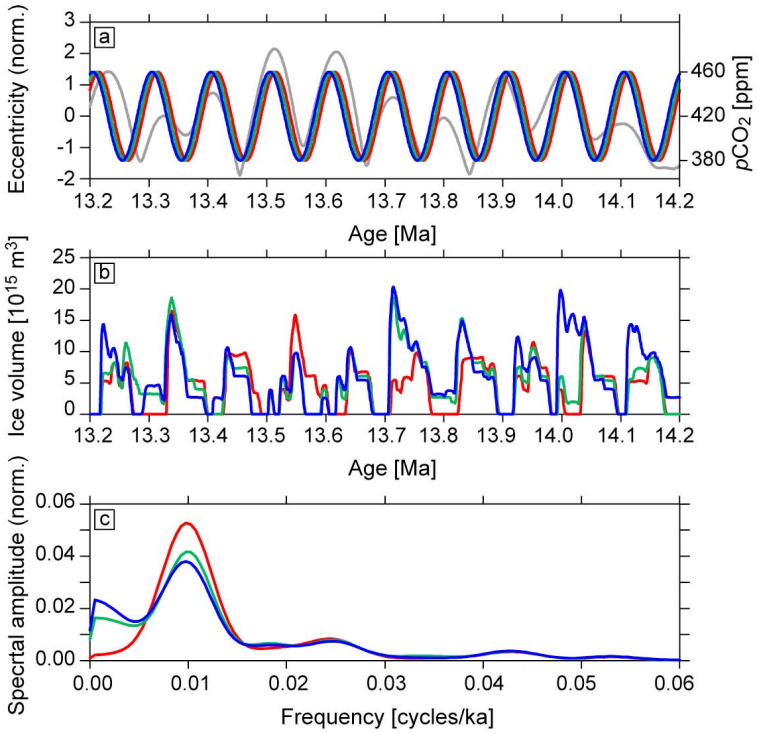

Fig. 8. Forced 100-ka pCO_2 cycles. **(a)** Normalized eccentricity (grey). **(b)** and **(c)** pCO_2 scenarios (colors) with mean levels of 420 ppm and amplitude of 40 ppm. Maxima in pCO_2 are tuned to maxima in eccentricity (best fit in green). Resulting glacial-interglacial ice-volume cycles. Normalized power spectral densities, with a strong 100-ka periodicity. Spectral analyses were performed using function pwelch in MATLAB 7.3.0.

CPD
4, 859–895, 2008